Overlay metrological system for overlaid linear gratings by an interferoscatterometer

Deh-Ming Shyu and Mao-Hong Lu

Citation: Review of Scientific Instruments **76**, 085103 (2005); doi: 10.1063/1.1994920
View online: http://dx.doi.org/10.1063/1.1994920
View Table of Contents: http://scitation.aip.org/content/aip/journal/rsi/76/8?ver=pdfcov
Published by the AIP Publishing

Articles you may be interested in

K-edge and mirror filtered X-ray grating interferometers
AIP Conf. Proc. **1466**, 229 (2012); 10.1063/1.4742297

X-ray grating interferometry - Applications in metrology and wave front sensing
AIP Conf. Proc. **1466**, 23 (2012); 10.1063/1.4742264

Laser interferometric nanolithography using a new positive chemical amplified resist
J. Vac. Sci. Technol. B **25**, 2476 (2007); 10.1116/1.2800328

X-ray wavefront analysis and optics characterization with a grating interferometer
Appl. Phys. Lett. **86**, 054101 (2005); 10.1063/1.1857066

Image metrology and system controls for scanning beam interference lithography
J. Vac. Sci. Technol. B **19**, 2335 (2001); 10.1116/1.1409379

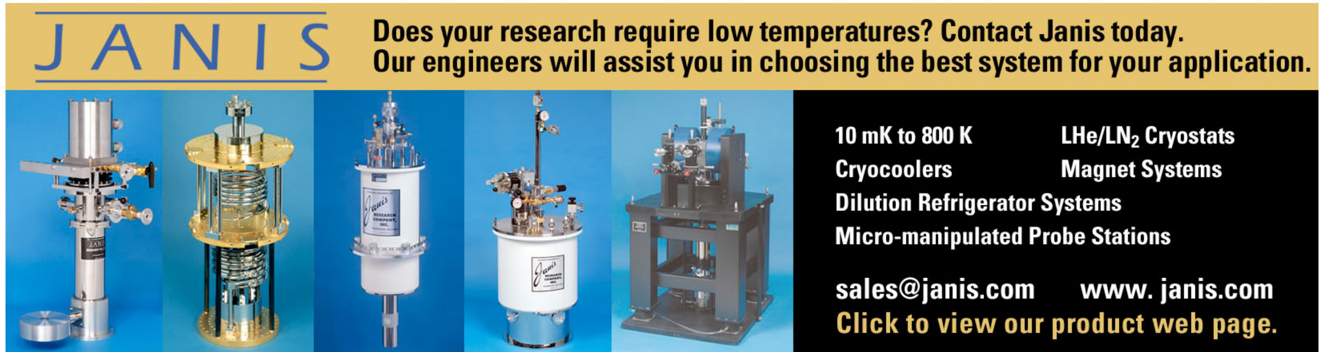

This article is copyrighted as indicated in the article. Reuse of AIP content is subject to the terms at: http://scitationnew.aip.org/termsconditions. Downloaded to IP: 140.113.38.11 On: Thu, 01 May 2014 02:56:28

HTML ABSTRACT + LINKS

REVIEW OF SCIENTIFIC INSTRUMENTS **76**, 085103 (2005)

Overlay metrological system for overlaid linear gratings by an interferoscatterometer

Deh-Ming Shyu[a] and Mao-Hong Lu[b]
Department of Photonics & Institute of Electro-Optical Engineering, National Chiao Tung University, 1001 Ta Hsueh Road, Hsinchu, Taiwan 300, Republic of China

(Received 20 April 2005; accepted 13 June 2005; published online 22 July 2005)

Interferoscatterometry is an optical measurement technology based on the analysis of light scattered and interfered from a periodic structure. In this work, first we build up a model for this system by the rigorous coupled wave analysis. With the model we calculate the diffractive efficiency of overlaid linear gratings with a mirror located in the incident region. Then, from the analyses of the overlaid linear gratings we obtain the best structure which has the highest sensitivity in the interferoscatterometry. Finally, we measure a sample and get experimental signatures. In order to get the overlay between the upper and lower grating, we compare the experimental signatures with theoretical signatures which are built in a library. The application of the interference technique on the scatterometry shows a higher sensitivity and a longer measurement range. © *2005 American Institute of Physics.* [DOI: 10.1063/1.1994920]

I. INTRODUCTION

The development of the semiconductor industry has created the need for reliable overlay metrology. According to a developmental report of the semiconductor technology by ITRS 2004 (International Technology Roadmap for Semiconductor), the pitch of 70 nm needs overlay control (accuracy) below 25 nm and overlay metrology precision below 2.5 nm. In the future, the pitch below 50 nm will need a metrological tool which has higher overlay control and precision to the overlay metrology. It is difficult to achieve by the conventional bright-field microscope because of the diffractive limit and optical aberrations.[1,2]

Takahiro *et al.*[3–5] proposed a heterodyne interference method instead of the bright-field microscope method. In their system, the upper and lower marks of the target were linear gratings which were overlaid each other and had the same pitches. The overlaid linear gratings are used as the alignment key. A *p*-polarization ray and an *s*-polarization ray were projected on the overlaid linear gratings and modulated at the same time. The diffractive beams from the overlaid linear gratings were subjected to frequency modulation. The frequency-modulated diffracted light beams were subjected to the heterodyne interference, and photoelectric conversion generated electrical signals so that the overlay between the upper and lower grating could be detected from phases of the two electrical signals. Another method[6,7] was proposed to measure the overlaid linear gratings with a scatterometry-based metrology. In this method the reflectance of the zero diffraction order from the overlaid linear gratings was measured by scanning the incident angle. Scatterometry has the advantages of being noncontact and nondestructive.

In order to obtain higher accuracy for the scatterometry-based overlay metrology, we must shrink the pitches of the upper and lower linear gratings.[8] Since the overlaid linear gratings have the reflection symmetry along the pitch direction when the overlay is zero, it will shorten the range of overlay measurement to half the pitch only. Huang[9] *et al.* used asymmetric overlay gratings to extend the range of overlay measurement from the half pitch to the whole pitch. But it also reduces the accuracy of the scatterometry-based overlay metrology.

In this article, we propose a method, interferoscatterometry, in which an interference of the zero order beam with a retroreflected+1 order beam is measured, as shown in Fig. 1. In this scheme we can get a higher accuracy and much longer measurement range than those in the scattermetry-based overlay metrology. Moreover, this system arrangement, named the interferoscatterometer, is simpler than that of an angular scatterometer, where the incident angle needs to scan.

II. RIGOROUS COUPLED WAVE ANALYSIS FOR THIS SYSTEM

Electromagnetic wave scattering from the periodic structure can be calculated by rigorous coupled wave analysis (RCWA).[10–13] In our simulation, the RCWA is modified for the mirror which is located in the incident region.

We follow Chateau's algorithm to describe the system in the matrix form

[a]Author to whom correspondence should be addressed; electronic mail: sidney.eo89g@nctu.edu.tw
[b]Electronic mail: mhlu@cc.nctu.edu.tw

 © 2005 American Institute of Physics

This article is copyrighted as indicated in the article. Reuse of AIP content is subject to the terms at: http://scitationnew.aip.org/termsconditions. Downloaded to IP: 140.113.38.11 On: Thu, 01 May 2014 02:56:28

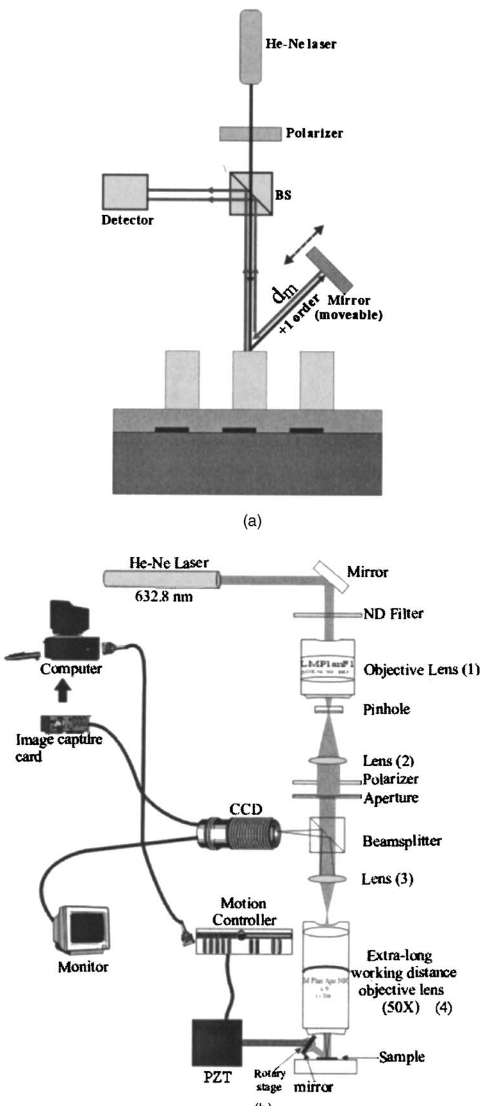

FIG. 1. The interferoscatterometer used in this study: (a) schematic diagram, and d_m is the distance from the mirror to the overlaid grating and (b) experimental arrangement. The light beam from the 632.8 nm He–Ne laser is spacially filtered and collimated by a pinhole and lenses (1) and (2). The collimated beam is polarized in TE mode by a polarizer and narrowed down by a telescope which consists of lenses (3) and (4). The retroreflection mirror is adjusted by a rotary stage and driven by a piezoelectric transducer (PZT). The interference intensity is measured by a CCD camera.

$$\begin{bmatrix} \vdots \\ f_F^{(i-\nu)} \\ \vdots \\ \vdots \\ b_F^{(i-\nu)} \\ \vdots \end{bmatrix} = [C(z_0)]^{-1} \left\{ \prod_{l=0}^{m-1} [G_l] \right\} [C(z_m)] \begin{bmatrix} \vdots \\ f_L^{(i-\nu)} \\ \vdots \\ \vdots \\ b_L^{(i-\nu)} \\ \vdots \end{bmatrix}, \quad (1)$$

where f_F, b_F, and f_L are the complex amplitude of the incident beam, reflective beam, and transmissive beam, respectively, and b_L is the complex amplitude of reflective beam from the transmissive region. Generally, b_L is set to be zero. $[C(z_0)]$ and $[C(z_m)]$ are the interface matrices in the incident region and transmissive region. $[G_l]$ is the characteristic matrix of the lth layer in the grating region, and is defined by

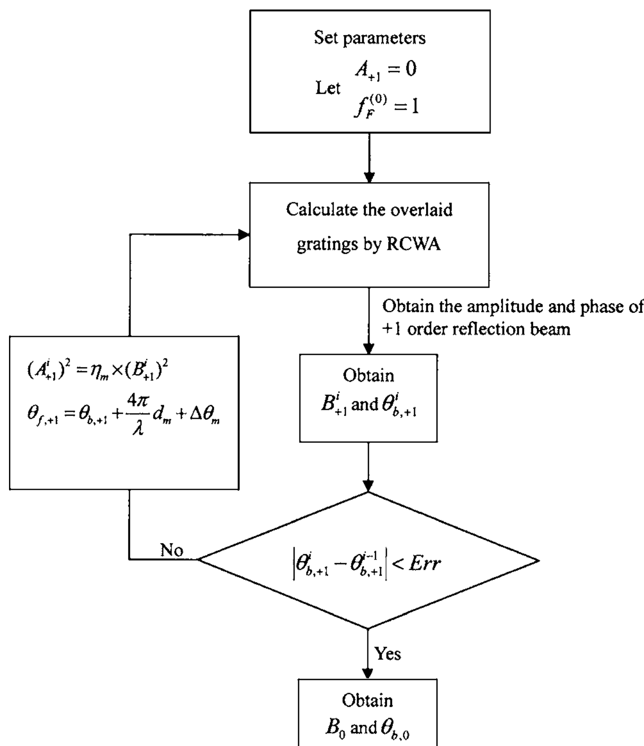

FIG. 2. Flowchart of calculation in the interferoscatterometer. The superscript i denotes the iterative number.

$$[G_l] = [P_l(z_l)]\exp\{-(z_{l+1}-z_l)[D_l]\} \times [P_l(z_{l+1})]^{-1}, \quad (2)$$

where $[P_l]$ and $[D_l]$ are the eigenvectors and the diagonal matrix of the eigenvalues, respectively, in the lth layer of the grating region.

We define the matrix of incident beams as

$$\begin{bmatrix} \vdots \\ f_F^{(-2)} \\ f_F^{(-1)} \\ f_F^{(0)} \\ f_F^{(+1)} \\ f_F^{(+2)} \\ \vdots \end{bmatrix} = \begin{bmatrix} \vdots \\ 0 \\ 0 \\ 1 \\ A_{+1}\exp(i\theta_{f,+1}) \\ 0 \\ \vdots \end{bmatrix}, \quad (3)$$

where $f_F^{(0)}=1$ is the normal incident beam and $f_F^{(+1)} = A_{+1}\exp(i\theta_{f,+1})$ is from the feedback of the output diffractive beam at the +1 order, and A_{+1} and $\theta_{f,+1}$ are the amplitude and phase of the retroreflected beam, respectively. Furthermore, the matrix of reflective beams can be defined as

$$\begin{bmatrix} \vdots \\ b_F^{(-1)} \\ b_F^{(0)} \\ b_F^{(+1)} \\ \vdots \end{bmatrix} = \begin{bmatrix} \vdots \\ B_{-1}\exp(i\theta_{b,-1}) \\ B_0\exp(i\theta_{b,0}) \\ B_{+1}\exp(i\theta_{b,+1}) \\ \vdots \end{bmatrix}, \quad (4)$$

where B_n and $\theta_{b,n}$ are the amplitude and phase of reflective beams at the n_{th} order, respectively. From Eqs. (3) and (4), A_{+1} and $\theta_{f,+1}$ are defined by

$$A_{+1}^2 = \eta_m \times B_{+1}^2,$$

This article is copyrighted as indicated in the article. Reuse of AIP content is subject to the terms at: http://scitationnew.aip.org/termsconditions. Downloaded to IP: 140.113.38.11 On: Thu, 01 May 2014 02:56:28

FIG. 3. Structure of the overlaid gratings, where L and S are line and space of the linear gratings, respectively.

$$\theta_{f,+1} = \theta_{b,+1} + \frac{4\pi}{\lambda} d_{m0} + \Delta\theta_m. \tag{5}$$

Here η_m is the reflectivity of the mirror, d_{m0} is the initial distance from the mirror to grating surface [see Fig. 1(a)], and $\Delta\theta_m$ is the phase shift due to the mirror moving. Using the iterative method, we can get the accurate amplitude A_{+1} and phase $\theta_{f,+1}$ of the feedback beam. Figure 2 shows the calculation flowchart. After the reflective beam $b_F^{(0)}$ with the amplitude B_0 and phase $\theta_{b,0}$ is determined, the reflection diffraction efficiency of the zero order $\eta_B^{(0)}$ is obtained by

$$\eta_B^{(0)} = |b_F^{(0)}|^2. \tag{6}$$

III. EXPERIMENTAL ARRANGEMENT AND SIMULATION

The experimental arrangement is illustrated in Fig. 1. A He–Ne laser is used as the light source. A polarizer is used to control the polarizations of the input beam. In this experiment, we only consider the *s* polarization [transverse electric (TE) mode]. The input beam is normally incident on the overlaid linear grating surface, and the +1 order diffractive beam is retroreflected to the overlaid linear gratings by a mirror. Interference happens between a reference beam and a modulation beam, where the reference beam is referred to the zero order diffractive beam and the modulation beam is referred to the +1 order diffractive beam reflected by the mirror. Finally, the interference intensity is measured by a charge coupled device (CCD) camera.

The interferoscatterometry as a metrology technique is used to determine the geometric parameters and the overlay between the upper and the lower linear gratings by the efficiency measurements of the light diffracted by the overlaid linear gratings. A schematic diagram of the sample used in this experiment is shown in Fig. 3. On a silicon substrate, two layers with linear grating structure are overlaid and in-between a thin film layer is deposited. An offset bias between the upper and the lower linear gratings is preset in order to have a maximum sensitivity of overlay metrology. The part of the overlay we are concerned with is the dislocation (ε) arising from misalignment in the process. The total overlay for the overlaid linear gratings is defined as Δx=offset bias $+\varepsilon$. In Fig. 3 the L and S denote the linewidth and line spacing of the linear gratings, respectively, and the geometric parameters of the sample are listed in Table I.

TABLE I. Geometric parameter of the sample.

	Material	thickness	n	k
Top layer	Photoresist	850 nm	1.624	0
Inter layer	Polysilicon	200 nm	3.926	0.059
Bottom layer	SiO_2	50 nm	1.463	0.000
Substrate	Silicon	—	3.867	0.020

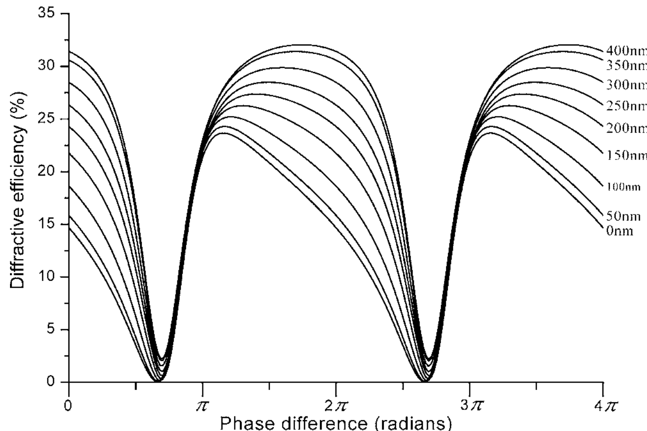

FIG. 4. Diffractive efficiency vs phase difference at pitch=800 nm, where the x axis gives the phase difference and y axis represents the diffractive efficiency.

If we take the $L/S=1/1$, pitch=800 nm, offset bias =0 nm, and λ=633 nm, the results of simulation are shown in Fig. 4, where the x axis gives the optical path difference change caused by the mirror moving and the y axis represents the diffractive efficiency of zero order. Signatures corresponding to overlay from 0 to 400 nm are shown in Fig. 4. For example, the 150 nm signature means the overlay is 150 nm. A maximum efficiency difference between the two adjacent signatures occurs at a certain phase difference. For example, if the overlay is in the range from 50 to 100 nm, the maximum efficiency difference is 2.8715% at a phase difference of 0.178π rad. The maximum efficiency differences for the overlay from 0 to 400 nm with an interval of 50 nm are listed in Table II, where we find the largest one is 3.3368% corresponding to the overlay from 100 to 150 nm. Thus, we

TABLE II. Phase difference vs the maximum efficiency difference for a 50 nm range. The phase difference is calculated from the optical path difference caused by the mirror moving.

Overlay (nm)	Maximum efficiency difference (%)	Phase difference (rad)
0–50	1.1910	0.122π
50–100	2.8715	0.178π
100–150	3.3368	0.233π
150–200	2.7563	0.250π
200–250	2.2571	0.256π
250–300	2.4712	0.294π
300–350	2.5014	0.322π
350–400	0.9243	0.256π

This article is copyrighted as indicated in the article. Reuse of AIP content is subject to the terms at: http://scitationnew.aip.org/termsconditions. Downloaded to IP: 140.113.38.11 On: Thu, 01 May 2014 02:56:28

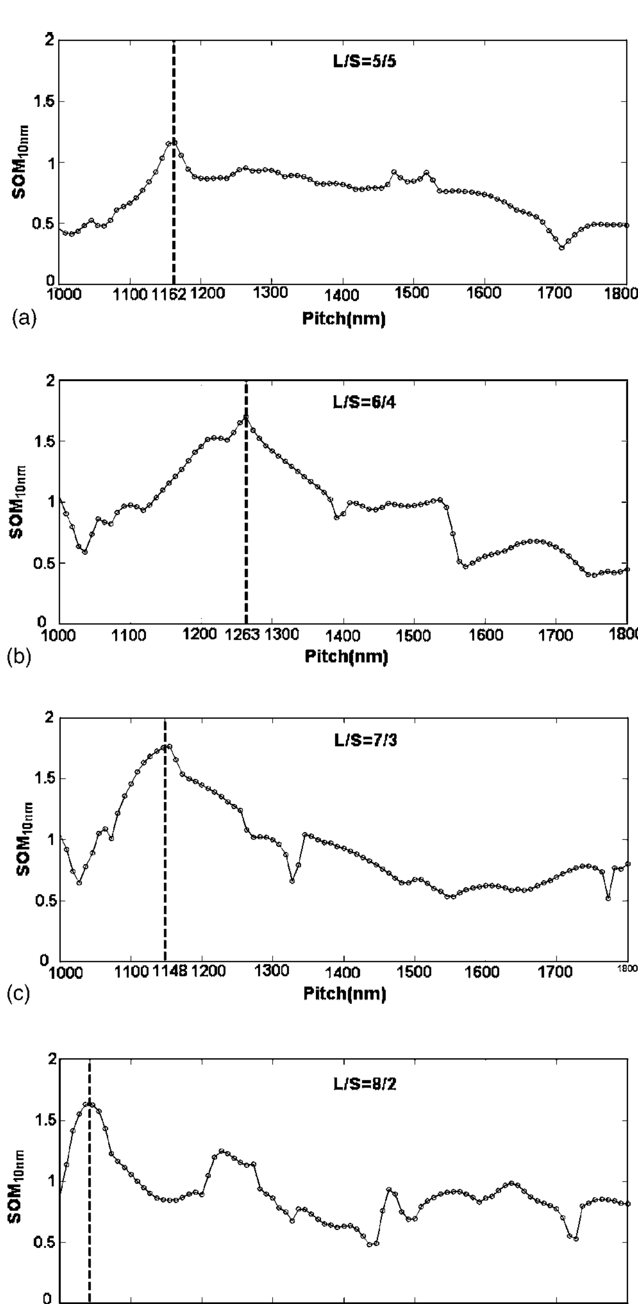

FIG. 5. Simulation results of optimizing parameters in the long range. The pitch of the grating changes from 1000 to 1800 nm with the interval of 10 nm and the L/S ratio changes from $L/S=5/5$ to 8/2. The peak location of $SOM_{10\ nm}$ moves from pitch=1160 nm (a) to pitch=1260 nm (b) and then goes back to pitch=1040 nm (d). The optimum $SOM_{10\ nm}$ is found at pitch=1150 nm (c).

can preset an offset bias between 100 and 150 nm for overlaid linear gratings to get the maximum sensitivity of the overlay metrology. In our simulation, the sensitivity of the overlay metrology ($SOM_{10\ nm}$) is referred to the global maximum value of the efficiency difference for the interval of 10 nm of the overlay between the upper and lower linear grating. Therefore, in Table II, the $SOM_{10\ nm}$ is 0.667 (the value of 3.3367% must be divided by 5, corresponding to the interval of 10 nm of the overlaid linear gratings).

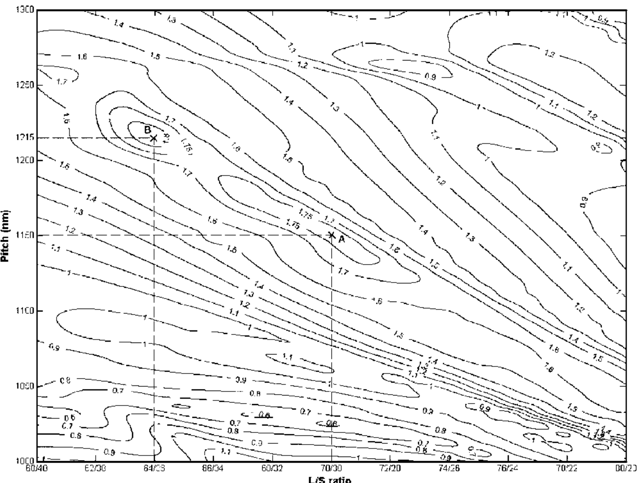

FIG. 6. Simulation results of optimizing parameters in the short range. The pitch changes from 1000 to 1300 nm with an interval of 5 nm and the L/S ratio changes from 60/40 to 80/20. The maximum value of $SOM_{10\ nm}$ is 1.8287 at point B ($L/S=64/36$, pitch=1215 nm). Point A is the submaximum value of $SOM_{10\ nm}$, which is from optimizing parameters in the long range [see Fig. 5(c)].

IV. OPTIMIZING THE PARAMETERS

In the process of making linear gratings, we can optimize the parameters of linear gratings for higher sensitivity. The parameters which could change without any effect on the process of making chips are the pitches and L/S ratio of the overlaid gratings. We sample the total range of the interested parameters by searching the grid and find the optimum solution range. Then, we shrink the searching range of parameters and increase the sampling resolution. Finally the optimum parameters could be found.

For the structure of Fig. 3 we change the pitch from 1000 to 1800 nm with the interval of 10 nm and the L/S ratio from $L/S=5/5$ to 8/2.The simulation results are shown in Fig. 5, where the x axis is the pitch of linear gratings and the y axis is the $SOM_{10\ nm}$. As the L/S ratio changes from $L/S=5/5$ to 8/2, the peak location of $SOM_{10\ nm}$ moves from pitch=1160 to 1260 nm and then goes back to pitch =1040 nm. The maximum value of $SOM_{10\ nm}$ is 1.76 if the $L/S=7/3$ and pitch=1150 nm. In order to find more accurate parameters, we shrink the searching range of simulation. Then, we change the pitches from 1000 to 1300 nm with intervals of 5 nm and the L/S ratio of simulation from 60/40 to 80/20. We find that the maximum value of $SOM_{10\ nm}$ becomes 1.8287 at $L/S=64/36$ and pitch=1215 nm. Figure 6 is the contour map of calculation. We take the initial value at point A and find the final value at point B after calculation

TABLE III. Optimum parameters of overlaid gratings for the interferoscatterometer and the angular scatterometer.

	Pitch (nm)	L/S ratio	Offset bias (nm)	
Interfero-scatterometer	1215	64/36	300	at phase difference $=1.667\pi$ rad
Angular scatterometer	460	48/52	395	at angle=14.3°

This article is copyrighted as indicated in the article. Reuse of AIP content is subject to the terms at: http://scitationnew.aip.org/termsconditions. Downloaded to IP: 140.113.38.11 On: Thu, 01 May 2014 02:56:28

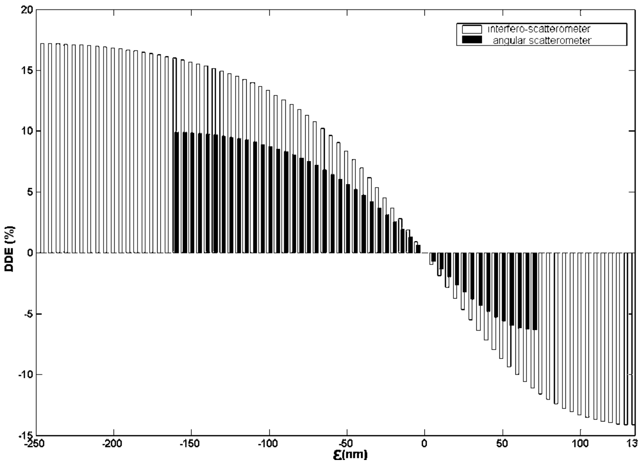

FIG. 7. The difference of diffractive efficiency (DDE) vs dislocation ε for two systems. The x axis, ε, is the dislocation caused by the misalignment in the process. The distance from −250 to 135 nm and from −160 to 70 nm are the available measurement dislocations for interferoscatterometer and angular scatterometer, respectively. The y axis is the DDE defined as DDE $=\mathrm{DE}_{\varepsilon}-\mathrm{DE}_{\varepsilon=0}$, where $\mathrm{DE}_{\varepsilon}$ is the diffractive efficiency at ε.

as shown in Fig. 6. The value at point B indicates the optimum parameters of the grating structure is in the range of pitch from 1000 to 1800 nm and for all L/S ratios.

Finally, we compare the sensitivity and the measurement range of this interferoscatterometer with those of the angular scatterometer. The optimum parameters for the two scatterometers are listed in Table III. The simulation results are shown in Fig. 7, where the x axis is ε which denotes the overlay exclusive of the offset bias, and the y axis is the difference of diffractive efficiency (DDE) defined as DDE $=\mathrm{DE}_{\epsilon}-\mathrm{DE}_{\varepsilon=0}$, where $\mathrm{DE}_{\varepsilon}$ is the diffractive efficiency at ε. The interferoscatterometer represented by white bars has a measurement range from −250 to 135 nm. The angular scatterometer represented by dark bars has a measurement range from −160 to 70 nm. So the measurement range of the interferoscatterometer is 67.4% larger than that of the angular scatterometer. The sensitivities in a short range of overlay are shown in Fig. 7, where the ε range is from +50 to −50 nm. In this range, the average value of the DDE is 4.9% for the interferoscatterometer and 3.3% for the angular scatterometer. Thus, the sensitivity of the interferoscatterometer is 47.3% larger than that of the angular scatterometer in the ε range from +50 to −50 nm as shown in Fig. 8.

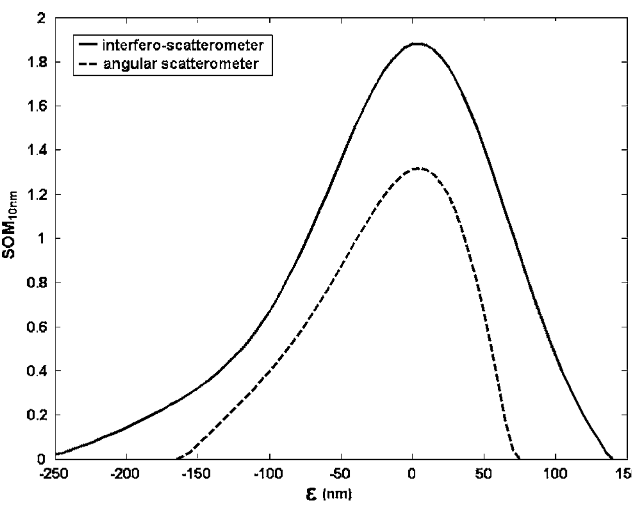

FIG. 8. The sensitivity of the interferoscatterometer and the angular scatterometer.

TABLE IV. The parameters of the overlaid gratings for measuring.

	Material	Thickness	Reflective index
Upper grating	PR	789.30 nm	1.624
Inter layer	Polysilicon	102.48 nm	$3.926-0.059i$
Lower grating	SiO_2	49.85 nm	1.463
Substrate	Si	—	$3.867-0.020i$

V. EXPERIMENT AND RESULTS

We fabricated a sample for tests of the interferoscatterometer. The parameters of the upper and lower linear gratings are listed in Table I for the material and thickness and the optimum parameters of the gratings designed for in the interferoscatterometer are shown in Table III. However, after fabrication, we find that the real structures of the gratings are a little different from the designed structures. The real parameters of the structures were measured by atomic force microscopy (AFM) and ellipsometer and are listed in Table IV. The size of the sample is 85 μm $\times$ 65 μm, which is big enough to meet the infinite boundary condition.[14] We measured the overlay of the sample with the interferoscatterometer.

The sample was measured consecutively 20 times in order to obtain the repeatability of the interferoscatterometry overlay measurements. The distribution of the overlay is from 432 to 435 nm and the peak is at 433 nm. The precision (3σ, σ is the standard deviation) of the interferoscatterometry measurement is 1.95 nm. The measured signature and the result of RCWA fitting for the mirror moving distance of four periods are shown in Fig. 9. In this figure, the real circles are the values measured by the interferoscatterometer and the real line is the fitting result by the RCWA. The method that we used for extraction of the overlay is the library-based methodology. First, linear gratings data, thin-film data, and sidewall angle data are used to obtain a collection of structures for the library-based methodology. Then, we can calculate and create the library of signatures of the diffractive efficiency from the collected structures by the RCWA. Finally, we calculate the root mean square (rms)

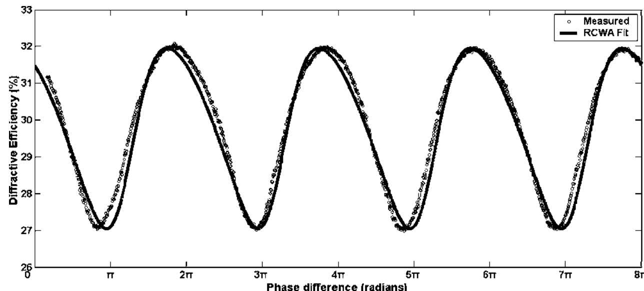

FIG. 9. The measurement result of the sample. The full line is the result of RCWA fitting for $\Delta x=433$ nm, and the circles are the values measured by the interferoscatterometry.

This article is copyrighted as indicated in the article. Reuse of AIP content is subject to the terms at: http://scitationnew.aip.org/termsconditions. Downloaded to IP: 140.113.38.11 On: Thu, 01 May 2014 02:56:28

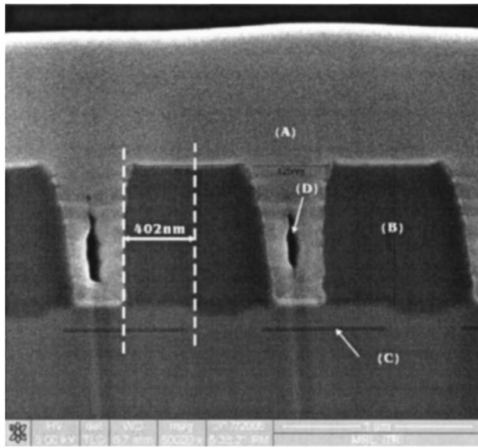

FIG. 10. The cross section of the sample measured with SEM. The layer (A) is used to protect the PR when making the cross section of the sample. The layer (B) is the PR and the layer (C) is the SiO_2. A hole (D) was produced when the layer (A) was spread on the PR. The total overlay is 402 nm.

between the measured signature and the library signatures and find the closest signature in the library to the measured signature. The overlay, Δx, of the sample which is extracted from the library-based methodology is 433 nm and then the ε is 133 nm.

After the sample was measured by the interferoscatterometer, we observed the crosssection of the sample with scanning electron microscope (SEM). The picture taken from SEM is shown in Fig. 10, from which a total overlay of 402 nm can be seen. There is a difference of 31 nm from the result given by our library-based methodology. The error could be mainly from the fact that we do not collect enough structures in the library to approach the measured signature exactly. For example, the sidewall angle in the library is from 0° to 5°, but the shape of sidewall is supposed to be straight and symmetric. In fact, the sidewall is bent and asymmetric as shown in Fig. 10.

ACKNOWLEDGMENTS

This work was supported by National Measurement Laboratory, the Industrial Technology Research Institute. The authors are grateful to Chun-Hung Ko and Dr. Yi-sha Ku for providing the samples and Dr. Shen-Chuan Lo for measurement with SEM.

[1] J. W. Goodman, *Introduction to Fourier Optics* (McGraw–Hill, New York, 1996), Chap. 6.
[2] M. Born and E. Wolf, *Principles of Optics* (Cambridge University Press, Cambridge, 1999), Chap. 9.
[3] N. Magome and Y. Ichihara, U.S. Patent No. 4,710,026 (1987).
[4] T. Matsumoto and N. Nose, U.S. Patent No. 5,369,486 (1994).
[5] T. Matsumoto, U.S. Patent No. 5,559,598 (1996).
[6] R. E. Chappelow and L. P. Hayes, U.S. Patent No. 4,757,207 (1988).
[7] W. Yang, L. W. Roger, and S. Rabello, Proc. SPIE **5038**, 200 (2003).
[8] E. M. Drege, R. M. Al Assad, and D. M. Byrne, Proc. SPIE **4689**, 151 (2002).
[9] H. T. Huang, G. Raghavendra, A. Sezginer, and K. Johnson, Proc. SPIE **5038**, 126 (2003).
[10] T. K. Gaylord and M. G. Moharam, Proc. IEEE **73**, 894 (1985).
[11] E. N. Glytsis and T. K. Gaylord, J. Opt. Soc. Am. A **4**, 2061 (1987).
[12] M. G. Moharam, E. B. Grann, and D. A. Pommet, J. Opt. Soc. Am. A **12**, 1068 (1995).
[13] N. Chateau and J. P. Hugonin, J. Opt. Soc. Am. A **11**, 1321 (1994).
[14] K. Hirayama, E. N. Glytsis, and T. K. Gaylord, J. Opt. Soc. Am. A **14**, 907 (1997).

This article is copyrighted as indicated in the article. Reuse of AIP content is subject to the terms at: http://scitationnew.aip.org/termsconditions. Downloaded to IP: 140.113.38.11 On: Thu, 01 May 2014 02:56:28